Eur. Phys. J. E (2015) **38**: 130
DOI 10.1140/epje/i2015-15130-4

THE EUROPEAN PHYSICAL JOURNAL E

Regular Article

Role of adhesion between asperities in the formation of elastic solid/solid contacts

L. Dies, F. Restagno, R. Weil, L. Léger, and C. Poulard[a]

Laboratoire de Physique des Solides, CNRS, Univ. Paris Sud, Université Paris-Saclay, 91405 Orsay Cedex, France

Received 15 July 2015 and Received in final form 23 October 2015
Published online: 23 December 2015 –

Abstract. We investigated the formation of a contact between a smooth sphere of elastomer and a micro-patterned elastomer substrate. We focussed our attention on the transition between a contact only established at the top of the pillars, and a mixed contact with a central zone of full contact surrounded by a top contact corona, which was observed when the normal load was increased. The full contact zone always nucleated with a finite radius, and the transition appears to be a first-order transition, with a hysteresis due to the creation of an adhesive zone between the pillars. We propose to include the effect of the new inter-pillar adhesion to produce a realistic treatment of the mechanics of these complex contacts. This new approach quantitatively accounts for the evolution of the observed jump in the radius of the full contact with the geometrical parameters of the pattern.

1 Introduction

When two solids are put into contact, the roughness of the two contacting surfaces plays a crucial role in determining whether adhesion will develop. Roughness of the two contacting surfaces prevents development of full intimate contact between the two solids, despite the presence of attractive interactions (van der Waals forces). This phenomenon has drastic consequences for a number of important applications in which one wishes to control adhesion or friction. It is indeed intuitively obvious that the strength of an interface should depend on the actual surface of contact between the two contacting solids, simply because this surface of contact represents the surface on which molecular interactions can act. Since solids are always deformable, the roughness asperities can deform under an applied normal load, which implies that this resultant actual surface of contact should depend on the applied load. Detailed mechanical models have been developed to predict this dependence in the case of a single contact between a smooth sphere and a smooth plane, either for the case of no adhesion forces (Hertz description) or for the more realistic situation where adhesive contact is present (JKR contact). In both cases, the size of the contact is predicted (and observed) to increase with the applied normal load in a non-linear manner. This is why the Amontons-Coulomb's friction law, which points out that the friction force is proportional to the load, independently of the apparent contact area between two solids [1,2] has long remained a kind of unexplained paradox, until Bowden and Tabor [3] proposed that the Amontons-Coulomb's law was reflecting the role played by the asperities of the two solid surfaces. Due to roughness, the solids are only contacting on top of the asperities, with a resulting real contact area A_{real} much smaller than the apparent one, A_{app}. More specifically in the case of metallic surfaces, they proposed that due to the concentration of the normal load on these contacting asperities, they undergo plastic deformation which fixes the value of the real contact area [4], potentially leading to a real surface of contact proportional to the normal load, and thus to a friction force that is itself proportional to the normal load.

The exact evolution of the real area of contact with the normal load is however a delicate question, involving the mechanical properties of the solids (close to their respective surfaces), the exact geometry of the two surfaces, and the adhesion between the solids. Building precise predictions for the evolution of the real contact area between two solids as a function of the applied normal load thus appears as a major but complex issue, which remains not fully elucidated, despite significant progress made over the past 50 or 60 years.

Following the pioneering work by Bowden and Tabor, a lot of experimental and numerical studies have attempted to quantify and model the proportionality between the load and the real area of contact, starting from the *a priori* simpler case of elastic asperities, and progressively exploring more complex mechanical behaviours (plastic deformations). Hertz [5] first modelled the adhesiveless and frictionless contact between a smooth elastic sphere and

[a] e-mail: christophe.poulard@u-psud.fr

a smooth elastic planar solid (a model mono-asperity contact) and predicted a contact area increasing with the squeezing force F_N as $A \sim F_N^{2/3}$. The simplest model of randomly rough surfaces with spherical bumps of identical radius of curvature R and equal heights is known as the apparent paradox of elastic friction. It states that the real area of contact between rough surfaces should increase with the load, obeying a scaling $F_N^{2/3}$. This apparent paradox of friction in the case of elastic solids without plastic flows has been first understood by Archard [6], followed by Greenwood and Williamson [7] using a more sophisticated statistical models of asperities. Valid models in the case where $A_{\rm app} \ll A_{\rm real}$ have been recently reviewed by Zavarise *et al.* [8]. A different approach has been developed by Persson, taking into account the elastic coupling between asperities inside the contact region, allowing the contact between randomly rough surfaces up to full contact to be described [9,10].

The contact between elastic adhesive solids is more complex. An elastic sphere in adhesive contact with a flat substrate was first modelled by Johnson, Kendall and Roberts [11,12] who calculated the evolution of the contact area as a function of the normal load (a model mono-asperity adhesive contact). The so-called JKR theory has later been extended to random rough surfaces [13–16] either to understand adhesion or friction behaviours. The question of the contact formation between a sphere and a wavy surface has been initially studied by Johnson [17] but most of the effort has been carried out in the field of biomimetic surfaces, in order to control and predict adhesion forces. It has been shown that dividing a surface into sets of parallel soft asperities can significantly increase adhesion if the aspect ratio (height over diameter) of the asperities is high enough to increase its compliance, as it is the case for biomimetic surfaces based on fibrillar structures [18–25]. In fact, fibrillar structures have, *a priori*, two antagonistic effects: they are more compliant than the bulk solid, and can adapt to the surface roughness of the substrate on which they are put into contact, a factor which tends to increase adhesion, but they intrinsically produce a smaller area of contact than a fully adaptable continuous material able to produce a full real contact with the substrate, a factor which tends to decrease adhesion. This has been clearly shown for wrinkled surfaces: to modulate adhesion or friction properties, a gain in compliance has been achieved by using soft elastomers and changing the contact area by forming either top or full contact [26–28]. For top contact, a decrease of adhesion has been observed, due to the decrease of real contact area, whereas full contact was conducive to an increase in adhesion.

In the present study, we take advantage of recent advances in the understanding of the contact mechanics between model micro-patterned surfaces to experimentally analyse and quantify the role of the adhesion which develops between the fibrillar structures at sufficiently large applied normal load, in the formation of contact. We chose small cylindrical fibrils with an aspect ratio smaller than one, to avoid their bending or buckling. Such small fibrils are called pillars in this paper. We used regular arrays of elastic micro-pillars, as previously used by Wu *et al.* [29], Verneuil *et al.* [30] and later by Degrandi *et al.* [31], in contact with a millimetric smooth elastic sphere. A common observation of these authors is that tall pillars can give a partial contact, with the smooth surface only touching the top of the pillars. Due to adhesion, short pillars are not able to prevent the two surfaces from establishing a full contact, which occurs at least in the central part of the apparent contact area. This kind of contact is called mixed contact (a central full contact area surrounded with a corona of top contact). A transition from only top contact to mixed contact is observed either by decreasing the height of the pillars at fixed load, as investigated by Verneuil *et al.* [30], or, at a sufficient height of the pillar, when increasing the applied normal load, as shown by Degrandi-Contraires *et al.* [31]. More precisely, Jin *et al.*predicted and observed experimentally the dependence of the threshold normal load characterising the transition from top to mixed contact on the pattern geometry and on the elastic properties of the materials in contact. Finally, Wu *et al.* [29] have shown that the precise fraction of full contact within the mixed contact area allows one to tune the friction properties of these micro-patterned contacts. On rippled elastic surface, Jin *et al.* [32] observed a similar evolution of the nature of the contact, but with a continuous transition from partial to full contact as a result of the 2D geometry.

A quite surprising result of [31] is that, when crossing the transition from partial to full contact, the full contact nucleates and suddenly jumps to a finite radius of full contact. This implies the onset of new adhesive energy contributions, which develop without affecting the apparent contact area. In the present article, after a rapid description of the details of the experimental setup and of the materials, we shall present a series of experimental data exploring the development of the full contact when crossing the threshold load. We propose a mechanical model of these complex contacts, based on a balance between adhesion and elastic deformation. This new approach quantitatively accounts for the jump in the radius of the full contact at the transition, and also for the further increase of this radius when further increasing the applied normal load. This description can thus be used to identify the pertinent parameters controlling this transition. This opens the route for the creation of versatile materials with selective adhesion and friction properties.

2 Materials and methods

2.1 Patterned surfaces

The micropatterned solid surfaces were replicated by molding, by using a silicon wafer with an etched resist layer as a mold. This mold was obtained through standard electron beam lithography techniques described in [33]. PDMS replicas were obtained by pouring in this mold a millimetre thick layer of silicone elastomer precursor mixed with a crosslinker, at a 10:1 ratio (Sylgard 184,

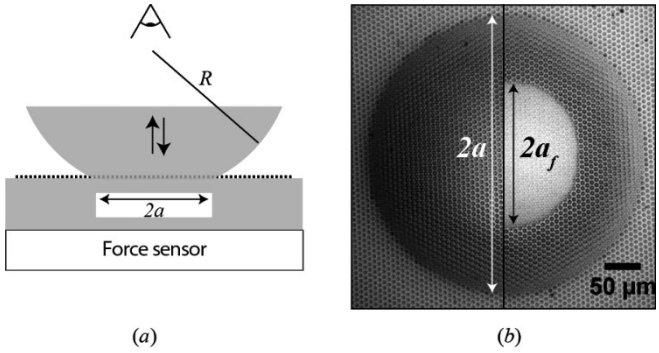

Fig. 1. (a): Schematic view of the sphere-plan JKR geometry. The substrate is linked to a force sensor and the lens is linked to a vertical motorized linear stage. The contact is observed through a long working distance microscope and monitored with a video camera (b): Top view of the contact between the lens and the patterned substrate for "top contact" (left) and "mixed contact" (right) just below (left) and just above (right) the transition.

Dow Corning), followed by a 24 h curing at 50 °C, and finally the crosslinked PDMS elastomer was peeled off from the mold. The elastic Young modulus of these substrates, $E_s = 1.8 \pm 0.1$ MPa, has been measured through classical JKR test on a smooth part of the substrate [12,34]. All data presented in this paper have been obtained with patterned surfaces made of regular hexagonal arrays of cylindrical pillars. The variable geometrical characteristics of such patterns included the height and the diameter of the pillars (respectively h and d), and their spacing that we have characterised by the mesh size of the array, i. The investigated diameters of pillars, d, were 4 μm and 6 μm. The mesh size, i, was varied in the range from 12 μm to 57 μm, and the height of the pillars, h, in the range from 0.5 μm to 3.5 μm.

2.2 Lens fabrication

The same elastomer was used to prepare small hemispherical lenses. These convex micro-lenses were obtained by the now classical method introduced by Whitesides and Chaudhury [35]: droplets of the reactive mixture were deposited on a glass slide covered by a SAM of perfluorinated silane to obtain a partially wetting substrate for PDMS. The same curing procedures as for the patterned substrates were applied to the droplets. The JKR test allowed us to measure their Young modulus as $E_l = 1.8 \pm 0.1$ MPa, similar to that of the patterned substrates.

The typical JKR geometry used to investigate the formation of the contact is schematically presented in fig. 1a, while a typical view of the contact is shown in fig. 1b, just below (left) and just above (right) the transition from top to mixed contact.

3 Experimental results

The contact, schematically presented in fig. 1(a), between a smooth elastomer lens and series of elastomer substrates patterned with regular hexagonal arrays of cylindrical pillars has been analysed experimentally in a lab-developed JKR test apparatus, described in detail in [34]. The evolution of the different contact radii (apparent and full contact) *versus* the applied normal load F, was continuously monitored though video microscopy.

As illustrated in fig. 1b, and as was reported in [31], contact of two different natures could be observed, depending on the applied load. For sufficiently small normal loads, "top contact" occurs, with the lens only touching the patterned substrate at the top of the pillars. The pillars thus remain fully visible all over the contact zone, as a result of air trapped in between the lens and the substrate at the base of the pillars, which gives a good optical contrast due to the large index of refraction mismatch between air and the silicone elastomer. At a given threshold load, named F_c, the nature of the contact suddenly changes with the rapid development, at a fixed load and fixed radius of apparent contact, of a contrasting central area of radius a_f. This central area, the so-called "full contact" area, corresponds to a supplementary contact between pillars, which then become hardly visible, because there is no air trapped between the pillars and the lens, and thus optical contrast is no longer present. This area of "full contact" remains always surrounded by a corona of "top contact" indicating that at the periphery of the apparent contact, the local force experienced by the pillars is lower than F_c. When the load is increased above F_c, both a and a_f continue to increase smoothly.

The evolutions of the full contact radius a_f (circle symbols) and of the overall apparent contact radius a (cross symbols), are reported in fig. 2 for different values of the fraction of surface occupied by the pillars, which we have characterised with the parameter ϕ. For the hexagonal geometry used here

$$\phi = \left(\pi/2\sqrt{3}\right)(d/i)^2. \quad (1)$$

For the full contact radius, a_f, all curves in fig. 2 exhibited a jump from zero to a finite value when crossing the threshold load. This clear jump allowed one to precisely determine the threshold load F_c. We note in fig. 2 that the apparent radius of contact, a, does not change when the full contact nucleates. This may seems surprising with regard to the large new adhesion contribution associated with the newly developed large surface of contact.

Data in fig. 2 clearly showed that the amplitude of the jump for a_f increases when ϕ increases, *i.e.* when the mesh size decreases at a fixed diameter of the pillars.

The contact formation and this abrupt jump of the full contact radius have to be understood in detail in order to use patterning as a tool to control friction and adhesion.

More generally, the smooth/micro-patterned silicone elastomer system used here appeared to be a quite convenient model system to investigate the relative roles of adhesion and elasticity on the formation of rough contacts: first, only elastic deformations are present, second the PDMS/PDMS adhesion energy is well known, and third, the geometrical parameters of the pattern can be varied in a wide and controlled range.

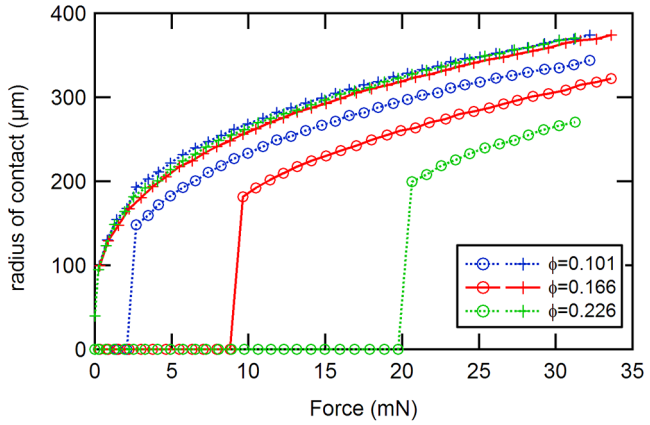

Fig. 2. Experimental evolution of the radius of contact as a function of the vertical force for different surface densities of pillars φ. The cross symbols correspond to the evolution of the apparent contact radius a, the circles correspond to the full contact radius a_f.

Compared to a smooth contact, the supplementary elastic energy associated with the compression of the pillars and with the deformations of both the underlying substrate and the lens between the pillars, is unfavorable for the creation of a full contact. On the contrary, the additional adhesion, which develops between the pillars inside the zone of full contact tends to pull lens and substrate into more intimate contact, and thus tends to increase the radius of full contact as soon as the threshold is reached. The aim of the analysis that we present below is to model the balance between the corresponding elastic and adhesion energies, focusing on the prediction of the amplitude of the jump in the radius of full contact at threshold loading.

4 Mechanical modelling of the patterned/smooth contact:

Let us first remind the reader of the simplest model that we have developed in [33] to predict the threshold force for the onset of full contact when an elastomer lens is pushed into contact with a micro-patterned elastomer substrate. The critical force can be deduced from a deformation criterion: to nucleate the full contact, lens and substrate need to touch in between the pillars. This means that the algebraic sum of the deformations of the lens, the substrate and the central pillar (fig. 3) which is compressed and supports the local maximum stress, is equal to the height of the pillars, h.

More precisely, the local deformations of both lens and substrate (respectively ξ_s^c and ξ_l^c) at the centre of the contact can be expressed as a function of the local stress σ_0: they correspond to indentation profiles by the cylindrical pillar [12,32]

$$\xi_{s,l}^c = \frac{3d}{2\pi E_{s,l}} \sigma_0 \cdot f_c(\phi). \tag{2a}$$

The correcting function, $f_c(\phi)$, previously introduced in [31], takes into account the perturbation of the deformation field associated to coupling between pillars when they are close enough, and goes to one for pillars separated at large distances.

The compression of the central pillar is also given in a straightforward manner by [12]

$$\delta = \frac{\sigma_0 h}{E_s}. \tag{2b}$$

The deformation criterion can thus be expressed as

$$\xi_l^c + \xi_s^c = h - \delta. \tag{2c}$$

By substituting into eq. (2c) the expressions of the deformations *versus* the local stress (eqs. (2a) and (2b)) one can express the threshold stress σ_c as a function of the geometric and elastic parameters of the system. Taking into account $E_s = E_l = E$ and assuming non-coupled pillars ($f_c(\phi) = 1$), this threshold stress is thus simply

$$\sigma_0 = hE\left(\frac{3d}{\pi} + h\right)^{-1} \equiv \sigma_c. \tag{3}$$

Using the classical expression for the normal stress at the centre of a Hertz profile: $\sigma_0 = 1/(\phi\pi)(FK^2/R^2)^{1/3}$, where $K = 4E/6(1-\nu^2)$ and ν is the Poisson ratio of the materials, that yielded the critical force. The ϕ factor took into account the concentration of the normal load at the top of the pillars. We have shown that this criterion was indeed able to correctly account for the observed evolutions of the threshold force *versus* the geometrical parameters of the pattern [31]. Alone, it did not however allow one to locate the external limit of the zone of full contact, even if it appears plausible to assume that at the limit of the zone of full contact, a_f, the deformation criterion (2c) should hold. To specify a_f from arguments similar to those used to define the threshold stress, an additional assumption on the stress profile was required. This was indeed a delicate point, since the development of the full contact zone, and the additional corresponding adhesion, may deeply affect the stress profile inside the contact zone. Assuming that a Hertz stress profile continued to apply, a simple prediction for the evolution of the radius of full contact with applied load could be made, but this prediction did not account for the observed jump in a_f at the threshold loading. The argument is as follows: if the normal load was progressively increased above the threshold, the critical stress for the onset of full contact will be achieved at a larger radius, a_f. Using the normal stress distribution in a Hertz contact, $\sigma(r) = \sigma_0(F)(1 - \frac{r^2}{a^2})^{1/2}$, and substituting that $\sigma(a_f) = \sigma_c$ one obtains

$$\frac{a_f^2}{a^2} = 1 - \left(\frac{F}{F_c}\right)^{\frac{2}{3}}. \tag{4}$$

This gave a smooth continuous increase of the radius of full contact from zero, and does not account for the nucleation of the full contact zone with a finite radius that was observed at threshold loading.

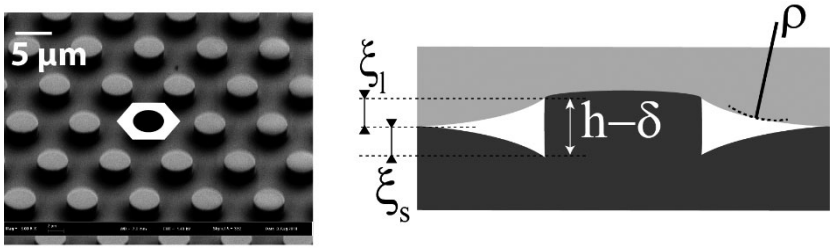

Fig. 3. Left: Scanning electron microscopy of a typical patterned surface. The area of the white portion of hexagon can be easily calculated: $S = \frac{3\sqrt{3}}{2} i^2(1-\phi)$. Right: Schematic representation of the lens, substrate and pillar when they are loaded at threshold, so that lens and substrate just touch. The definition of the different deformations δ, ξ_l and ξ_s is indicated, along with ρ, the local radius of curvature of the indentation profile.

We propose here to modify the deformation criterion describing the limit of the area of full contact, in order to take into account the additional adhesion that develops between the pillars when the full contact develops above the threshold.

As soon as lens and substrate touch between the pillars, the adhesion associated with the newly created surface of contact tends to further close the contact, and therefore will exert an additional compression at the interface. Experimentally, no change was found in the evolution of the apparent radius of contact, a when crossing the transition [31] as shown in fig. 2. This is a strong indication that the supplementary adhesion energy gained when forming the new full contact has been locally converted into other energies contributions, elastic energy and dissipation losses. We know from the investigations of the formation of the contact in the case of PDMS micro-lens on smooth PDMS, that the dissipation losses are not dominant, so that the balance between elastic energy and adhesion energy leads to a correct determination of the thermodynamic wok of adhesion for this PDMS/PDMS System [34]. We thus chose, in a first approximation, to omit the effects of dissipation.

Two elastic contributions corresponding to two "springs" can *a priori* be identified: a supplementary compression of the pillars inside the full contact zone (a modification of δ resulting from the new adhesion, that we call $\delta_{\rm adh}$) and additional indentations of the inter-pillar regions of the sphere and the substrate (an extra $\xi_{\rm adh}$) which are squeezed against each other due to the adhesion terms. The effect is cumulative, and every pillar and inter-pillar zone having passed the transition can contribute to an increase in the local deformation applied to the following pillars.

For the hexagonal array used in the present experiments, the additional adhesion energy for one pillar, $U_{\rm ad}$, is related to the work of adhesion W on the freshly created surface (fig. 3)

$$U_{\rm ad} = \left(\frac{3\sqrt{3}}{2} i^2 - \frac{3\pi}{4} d^2\right) W = \frac{3\sqrt{3}}{2} i^2 (1-\phi) W. \qquad (5)$$

This adhesion energy will be distributed over the two springs corresponding, respectively, to the compression of pillars and to the supplementary elastic deformations of the sphere and of the substrate. This last elastic contribution is not at all easy to evaluate. It corresponds to the formation of an adhesive contact in the interpillar zone, which is curved, not axisymmetric, and quite different from a simple JKR contact, due to the constraints imposed locally by the yet formed adhesive contacts on top of the pillars. Far from the edge of a pillar, the radius of curvature, ρ, just below the threshold loading, would be the local curvature of the indentation profile of an elastic solid by a flat punch, with ρ larger than R (fig. 3). If we were dealing with a simple JKR smooth elastic contact with a lens of radius ρ, an indentation in the micrometric range would produce a contact with a radius larger than a, and thus much larger than i, the inter-pillar distance. It is then plausible to assume, in a first approximation, that what prevents the development of a large contact is mainly the elastic over-compression of the pillars, $\delta_{\rm ad}$, and not the elastic deformations inside the inter-pillar zone. The additional elastic energy of compression of the pillars could be written as

$$U_{\rm el} = \frac{\pi E d^2}{8h} \delta_{\rm ad}^2. \qquad (6)$$

Balancing eqs. (5) and (6) and using eq. (1) for the dependence of ϕ on diameter and spacing of the pillars, led to $\delta_{\rm ad}$

$$\delta_{\rm ad} = \sqrt{\frac{Wh}{E}\left(\frac{1-\phi}{\phi}\right)}. \qquad (7)$$

The deformation criterion of eq. (2c) then became

$$\xi_l(a_f) + \xi_s(a_f) + \delta(a_f) + \delta_{\rm adh} = h, \qquad (8)$$

Using the expressions for $\xi_{l,s}$ and δ (eqs. (2a) and (2b)), and using a Hertz stress profile, which is valid at the loading threshold, with $\sigma_0 = \sigma_c$, we obtain

$$\sigma_c \sqrt{1 - \left(\frac{a_f}{a}\right)^2} \left(\frac{3d}{\pi E} + \frac{h}{E}\right) = h - \delta_{\rm adh}. \qquad (9)$$

This can be simplified using eq. (3)

$$\frac{a_f}{a} = \sqrt{1 - \frac{(h-\delta_{\rm ad})^2}{h^2}}. \qquad (10)$$

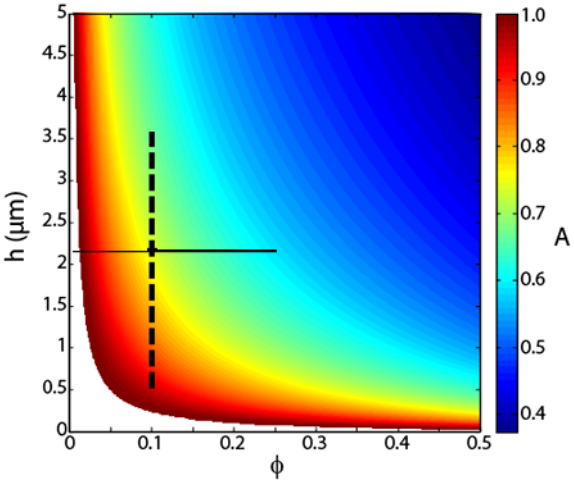

Fig. 4. Map representation of the evolutions of the amplitude A *versus* the height h of the pillars and the areal density φ, as predicted by eq. (11). The full line corresponds to fig. 5 (upper part) where experiments have been carried out with $h = 2.2\,\mu$m and varying ϕ. The dotted line corresponds to fig. 5 (lower part) where experiments have been carried out with $\phi = 0.1$ and varying h.

Combining eqs. (10) and (7) gave the variation of the amplitude of the jump in the radius of full contact at threshold, A, with the geometrical parameters of the pattern, the elastic modulus and the thermodynamic work of adhesion

$$A \equiv \frac{a_f}{a} = \sqrt{\frac{W}{Eh}\left(\frac{\phi-1}{\phi}\right) + 2\sqrt{\frac{W}{Eh}\left(\frac{1-\phi}{\phi}\right)}}, \qquad (11)$$

Figure 4 gave a map of the evolution of the amplitude of the jump in the radius of full contact at threshold (colour code on the right) *versus* ϕ and h, as deduced from eq. (11). This map showed that ϕ and h have approximately the same effect on A (almost symmetrical repartition of colors around $h = 10^{-5}\phi$ which correspond to the diagonal of the map). This result could also be deduced from eq. (11), taking the limit for $\phi \ll 1 : A$ then became proportional to $(h\phi)^{-1}$.

Comparison to experiments

The predictions of eq. (11) were compared to experiments in fig. 5(a) for the dependence *versus* the surface density of pillars and in fig. 5(b) for the height dependence. The smallest ϕ value corresponded to a large separation between pillars ($i = 57\,\mu$m). In this case, the critical force was low, the number of pillars under the contact became small, and the mixed contact appeared for a rather small radius of the apparent contact. A precise value of A then became difficult to measure, and the uncertainty on A for the smaller ϕ is of the same order of magnitude as the value itself ($\Delta A \sim 0.2$).

When the density of pillars was increased, the fraction of the area of full contact at the transition increased as well, in surprisingly good agreement with the model, without any adjustable parameter. The inclusion of the supplementary compression of the pillars associated to adhesion, as estimated though the balance between adhesion energy and elastic compression energy in eq. (11), captured well all the main characteristics of the observed jump in the radius of full contact.

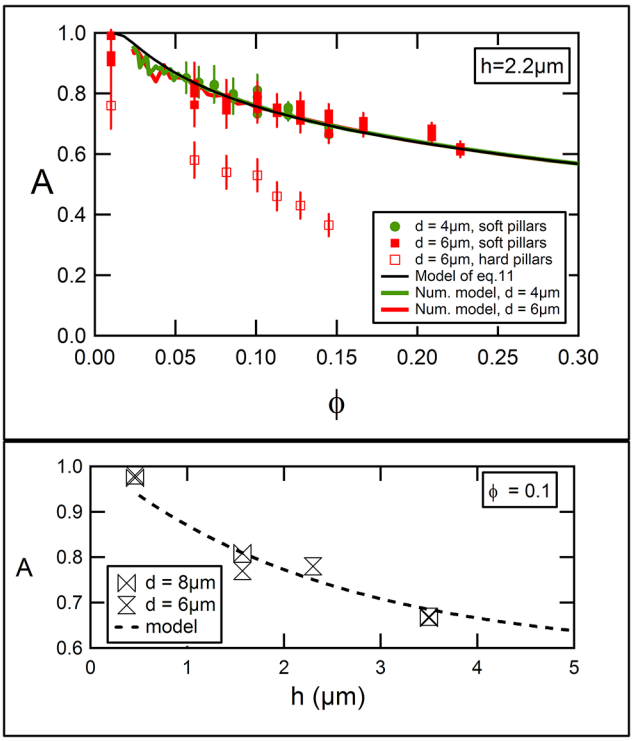

Fig. 5. (a) Evolution of the amplitude of the jump in the radius of full contact, A, at threshold, for two diameters (■ $d = 6\,\mu$m; • $d = 4\,\mu$m) for soft elastomer patterned substrates and one diameter (□ $d = 6\,\mu$m) for hard patterned substrates. The lines correspond to the analytical prediction of eq. (11) for "soft" contacts and the numerical models for a JKR stress distribution with coupling for $d = 4\,\mu$m and $d = 6\,\mu$m. (b) Experimental and analytical evolution of this amplitude *versus* the height for $\phi = 0.1$ for soft contacts.

Limitations of the model

The model leading to eq. (11) relied on several simplifications that we would now discuss, leaving aside initially the major and questionable assumption of an elastic contribution inside the new full contact dominated by the compression of the pillars.

First, we have assumed a Hertz distribution of stress under the contact, which means that we have neglected the adhesion at the top of the pillars during the contact formation (hypothesis 1). This assumption has been shown to be correct in the former evaluation of the threshold of full contact zone [33]. This weak adhesion at the top of the pillars could be taken into account using a numerical model.

A second assumption was to assume that the mechanical elastic coupling between the pillars could be neglected. Again, taking this coupling between pillars into account was previously achieved by numerical methods [31,33],

and could be implemented here with no effect on eq. (11), because only the overcompression of the pillars was taken into account in the evaluation of the of elastic energy (eq. (6)).

The present model should also break down at low ϕ. First, the assumption of a Hertz profile with a stress concentration at the top of the asperities should no longer be valid when the number of pillars under the contact becomes too small. Second, eq. (11) exhibits an interesting limit at low ϕ where A reaches the value $A = 1$. This corresponds to

$$\phi_c \sim \frac{W}{W + hE}. \tag{12}$$

Even if difficult to test experimentally (for the situations explored in this article ($W = 0.046\,\mathrm{mJ/m^2}$ and $E \sim 1\,\mathrm{MPa}$), $\phi_c \sim 0.013$, a low value where the hypothesis of a continuous Hertz profile of stress is not longer valid) this may indicate a change in contact and adhesive behaviour at low surface densities of pillars, which should be examined in more detail.

Numerical calculations

To try to further probe the analysis of the formation of this complex contact, the evolution of A had been computed numerically for a JKR stress distribution inside the contact before the threshold, still keeping the estimate of δ_{ad} given by eq. (7) and the hypothesis that the stress profile was kept equal to that of th JKR outside of the zone of full contact, down to a_f. In fig. 5(a), the numerical solutions computed for a JKR stress distribution plus coupling, and for the two diameters of pillars used in the experiments, were plotted as the red and green lines, for $d = 4\,\mu$m and $d = 6\,\mu$m respectively. These numerical solutions were fully superimposed with the analytical solution for the Hertz stress profile. This reflected the fact that, when in top contact, the effective adhesion energy was weakened compared to full contact, as only the tops of the pillars are involved in the contact.

Case of hard pillars

Even if eq. (11) fully accounted for the experimental data, without any adjustable parameters, it relied on a questionable hypothesis. We have assumed that the adhesion energy gained inside the zone of full contact was essentially converted into compression elastic energy of the pillars. We have totally neglected the elastic contributions associated to the deformations of the inter-pillar zone, despite the fact that these deformations are clearly present as the optical contrast of the pillars is lost in the full contact zone. We have also neglected potential dissipation terms. In order to gain some insight in the validity of these assumptions, we have performed some experiments with an elastomer lens in contact with a much harder patterned substrate, Araldite 2020 ($E \sim 1\,\mathrm{GPa}$) covered with an irreversibly adsorbed PDMS layer in order to keep W identical to the elastomer/elastomer experiments. In this case, the pillars were essentially incompressible and, if full contact appears, the corresponding adhesion energy should only be equilibrated by the deformation of the soft sphere between the pillars. A transition and the appearance of a zone of full contact at a given threshold load, along with a jump in the radius of full contact, were still observed in this case. The jumps in a_f appeared significantly smaller than in the "totally deformable" case, as shown by the corresponding green full symbols in fig. 5a.

An extension of the present model, taking correctly into account the elastic deformations of the lens due to the local closure of the contact between the pillars would be necessary to account for these experiments, and, in the fully deformable case, to more firmly justify eq. (11). This cannot be done analytically, because of the complex local deformed profiles of lens and substrate between the pillars. We are presently implementing such an approach, based on finite element analysis.

5 Conclusions

We have presented a series of experimental data for the evolution of the "full contact" radius when a patterned substrate is pushed into contact with a smooth elastomer lens in a JKR experiment. This work is the continuation of a previous paper, in which we reported and analysed how the critical load for the nucleation of a zone of full contact in the centre of the "top" contact area, was depending on the geometrical parameters of the pattern. The present work focused on the loading phase, was centred on the investigations and analysis of the evolution of the observed jump in the radius of full contact, which develops suddenly at the critical load, as a function of the mesh size i of the pattern, the diameter d of the pillars, and their height h. Extending our previous analysis describing the threshold critical load between top and mixed contacts, we have, analytically and numerically modelled, for the first time, the experimental data, taking into account the balance between adhesion and elastic energies inside the zone of full contact with some approximations. Indeed, the adhesion, which develops inside the zone of full contact as soon as the threshold load is attained tends to close the contact between the pillars, further compressing the pillars and thus pushing further past the limit whereby the zone of full contact appears. We showed that this additional adhesion is responsible for the sudden increase in the radius of full contact, while the radius of apparent contact remained constant. Even though approximations were used, the present analysis correctly accounts for all obtained data, without any adjustable parameter, and remained accurate even with variations in the density and height of the pillars.

This analysis demonstrated that apart from the height h, which has been usually considered as the parameter affecting the transition between top and mixed contact for a given applied load, ϕ, the surface density of pillars, can be used to adjust and control the nature of the contact.

We wanted to emphasise that the development of the central full contact zone occurred without any change in the radius of the corona of the top contact. This may seem surprising, as the development of the new inter-pillar contacts corresponds to a significant increase of adhesion

inside the full contact zone. This new adhesion, even if in part balanced against elasticity, should strongly modify the stress distribution under the contact, but this does not appear in the load *versus* radius curve. We wanted to point out that this behaviour is quite similar to what has been reported in a number of JKR experiments where adhesion was enabled to change under the contact, due to chemical reaction or to a progressive interdigitation between grafted polymer chains and the elastomer of the lens [36–39]. In all these experiments, the development of adhesion under the yet formed contact did not affect the contact radius, and was only revealed when unloading was performed.

Author contribution statement

The materials were prepared by LD and RW. All the experiments were carried out by LD and CP. Models were developed by LL, FR and CP. All the authors have contributed to the manuscript.

The authors greatly thank Jeremie Sanchez for experimental support. This work is supported by a public grant from the "*Programme blanc*" (ref. SIMI4-WAFPI-11-BS04-0030) overseen by the French National Research Agency (ANR).

References

1. B. Bhushan, *Modern Tribology Handbook* (CRC Press, 2001).
2. B. Bhushan, *Fundamentals of Tribology and Bridging the Gap Between the Macro-and Micro/Nanoscales* (Kluwer Academic, London, 2001).
3. F.P. Bowden, L. Leben, Philos. Trans A **239**, 1 (1939).
4. F. Restagno, J. Crassous, C. Cottin-Bizonne, E. Charlaix, Phys. Rev. E **65**, 042301 (2002).
5. H. Hertz, J. Reine Angew. Math. **92**, 156 (1881).
6. J.F. Archard, J. Appl. Phys. **24**, 981 (1953).
7. J.A. Greenwood, J.B.P. Williamson, Proc. Roy Soc. A **243**, 300 (1966).
8. G. Zavarise, M. Borri-Brunetto, M. Paggi, Wear **262**, 42 (2007).
9. B.N.J. Persson, Eur. Phys. J. E **8**, 385 (2002).
10. B.N.J. Persson, Surf. Sci. Rep. **61**, 201 (2006).
11. K.L. Johnson, K. Kendall, A.D. Roberts, Proc. R. Soc. Lond. Math. Phys. Sci. **324**, 301 (1971).
12. K.L. Johnson, *Contact Mechanics* (Cambridge University Press, Cambridge, 1987).
13. C.S. Hodges, L. Looi, J.A.S. Cleaver, M. Ghadiri, Langmuir **20**, 9571 (2004).
14. S. Yashima, V. Romero, E. Wandersman, C. Frétigny, M.K. Chaudhury, A. Chateauminois, A.M. Prevost, Soft Matter **11**, 871 (2015).
15. M. Benz, K.J. Rosenberg, E.J. Kramer, J.N. Israelachvili, J. Phys. Chem. B **110**, 11884 (2006).
16. A. Mitra, P. Sahoo, K. Saha, Tribol. Ind. **33**, 3 (2011).
17. K.L. Johnson, Int. J. Solids Struct. **32**, 423 (1995).
18. E. Arzt, S. Gorb, R. Spolenak, Proc. Natl. Acad. Sci. U.S.A. **100**, 10603 (2003).
19. M.D. Bartlett, A.B. Croll, D.R. King, B.M. Paret, D.J. Irschick, A.J. Crosby, Adv. Mater. **24**, 994 (2012).
20. J.Y. Chung, M.K. Chaudhury, J. R. Soc. Interface **2**, 55 (2005).
21. B. Bhushan, *Biomimetics: Bioinspired hierarchical-structured surfaces for green science and technology* (Springer, 2012).
22. A. Ghatak, L. Mahadevan, J.Y. Chung, M.K. Chaudhury, V. Shenoy, Proc. R. Soc. Math. Phys. Eng. Sci. **460**, 2725 (2004).
23. H. Zeng, N. Pesika, Y. Tian, B. Zhao, Y. Chen, M. Tirrell, K.L. Turner, J.N. Israelachvili, Langmuir **25**, 7486 (2009).
24. Y. Bai, C-Y. Hui, B. Levrard, A. Jagota, Langmuir **2015**, 7581 (2014).
25. C-Y. Hui, N.J. Glassmaker, T. Tang, A. Jagota, J. R. Soc. Interface **1**, 35 (2004).
26. Y. Rahmawan, C-M. Chen, S. Yang, Soft Matter **10**, 5028 (2014) DOI: 10.1039/C4SM00027G.
27. C.J. Rand, A.J. Crosby, J. Appl. Phys. **106**, 064913 (2009).
28. C.S. Davis, D. Martina, C. Creton, A. Lindner, A.J. Crosby, Langmuir **28**, 14899 (2012).
29. F. Wu-Bavouzet, J. Cayer-Barrioz, A. Le Bot, F. Brochard-Wyart, A. Buguin, Phys. Rev. E **82**, 031806 (2010).
30. E. Verneuil, B. Ladoux, A. Buguin, P. Silberzan, J. Adhes. **83**, 449 (2007).
31. É Degrandi-Contraires, A. Beaumont, F. Restagno, R. Weill, C. Poulard, L. Léger, EPL **101**, 14001 (2013).
32. C. Jin, K. Khare, S. Vajpayee, S. Yang, A. Jagota, C-Y. Hui, Soft Matter **7**, 10728 (2011).
33. C. Poulard, F. Restagno, R. Weil, L. Léger, Soft Matter **7**, 2543 (2011).
34. M. Deruelle, H. Hervet, G. Jandeau, L. Leger, J. Adhes. Sci. Technol. **12**, 225 (1998).
35. M.K. Chaudhury, G.M. Whitesides, Langmuir **7**, 1013 (1991).
36. P. Silberzan, S. Perutz, E.J. Kramer, M.K. Chaudhury, Langmuir **10**, 2466 (1994).
37. J.T.J. Koberstein, D.E.D. Duch, W. Hu, T.J. Lenk, R. Bhatia, H.R. Brown, J-P. Lingelser, Y. Gallot, J. Adhes. **66**, 229 (1998).
38. L. Léger, E. Raphaël, H. Hervet, in *Polymers in confined environments* (Springer, 1999) pp. 185–225.
39. H.R. Brown, Macromolecules **26**, 1666 (1993).